Published in final edited form as:

Connect Tissue Res. 2014 June ; 55(3): 205–216. doi:10.3109/03008207.2014.894997.

Topographical variations of the strain-dependent zonal properties of tibial articular cartilage by microscopic MRI

Ji Hyun Lee[1], **Farid Badar**[1], **David Kahn**[1], **John Matyas**[2], **Xianggui Qu**[3], **Christopher T. Chen**[4], and **Yang Xia**[1]

[1]Department of Physics and Center for Biomedical Research, Oakland University, Rochester, MI, USA

[2]Department of Comparative Biology and Experimental Medicine, Faculty of Veterinary Medicine, University of Calgary, Calgary, AB, Canada

[3]Department of Mathematics and Statistics, Oakland University, Rochester, MI, USA

[4]Department of Orthopaedic Surgery, University of Texas Southwestern Medical Center, Dallas, TX, USA

Abstract

The topographical variations of the zonal properties of canine articular cartilage over the medial tibia were evaluated as the function of external loading by microscopic magnetic resonance imaging (μMRI). T2 and T1 relaxation maps and GAG (glycosaminoglycan) images from a total of 70 specimens were obtained with and without the mechanical loading at 17.6 μm depth resolution. In addition, bulk mechanical modulus and water content were measured from the tissue. For the bulk without loading, the means of T2 at magic angle (43.6 ± 8.1 ms), absolute thickness (907.6 ± 187.9 μm) and water content (63.3 ± 9.3%) on the meniscus-covered area were significantly lower than the means of T2 at magic angle (51.1 ± 8.5 ms), absolute thickness (1251.6 ± 218.4 μm) and water content (73.2 ± 5.6%) on the meniscus-uncovered area. However GAG (86.0 ± 15.3 mg/ml) on the covered area was significantly higher than GAG (70.0 ± 8.8 mg/ml) on the uncovered area. Complex relationships were found in the tissue properties as the function of external loading. The tissue parameters in the superficial zone changed more profoundly than the same properties in the radial zone. The tissue parameters in the meniscus-covered areas changed differently when comparing with the same parameters in the uncovered areas. This project confirms that the load-induced changes in the molecular distribution and structure of cartilage are both depth-dependent and topographically distributed. Such detailed knowledge of the tibial layer could improve the early detection of the subtle softening of the cartilage that will eventually lead to the clinical diseases such as osteoarthritis.

Keywords

Cartilage; gadolinium; glycosaminoglycan; magnetic resonance image; mechanical modulus; strain; T1 relaxation time; T2 relaxation time

Correspondence: Yang Xia, Ph.D., Department of Physics and Center for Biomedical Research, Oakland University, Rochester, MI 48309, USA. Tel: +248 370 3420. Fax: +248 370 3408. xia@oakland.edu.

Introduction

Articular cartilage is a layer of load-bearing tissue in synovial joint that absorbs shock, distributes stress and provides a low-friction surface for joint motion. The tissue contains three major molecular constituents in its extracellular matrix: the collagen fibers that are organized into a depth-dependent zonal structure (commonly, SZ = the superficial zone, TZ = the transitional zone and RZ = the radial zone), the proteoglycan (PG) that determines the load-bearing property of the tissue, and a large amount of water molecules (1–3). Within the tibia of a single knee joint, the molecular constituents can have complex topographical variations in their interactions and concentrations at different surface locations, even just a few millimeters apart (4–8). Subtle modifications to the molecular environment and ultrastructure in cartilage could eventually lead to clinical diseases such as osteoarthritis (OA) (9,10).

Magnetic resonance imaging (MRI) has been widely used in research and diagnostics to visualize the morphological and molecular features of articular cartilage, because of its total non-invasiveness and high sensitivity to molecular environment. Among the commonly used MRI parameters, T2 relaxation time is sensitive to several molecular factors in cartilage including water content, PG content and collagen fibril organization (11–13). A unique feature of the T2 characteristics is its strong anisotropy in MRI, governed by the dipolar interaction between water protons and the external magnetic field (11). In contrast, T1 relaxation time in high fiend MRI of cartilage is nearly isotropic and much less sensitive to the influence of the dipolar interaction (11,14), although some clinical MRI studies at 1.5 T observed the variation of T1 with the tissue depth (15,16). One approach to utilize T1 in cartilage MRI is to soak/inject the paramagnetic contrast agents such as gadolinium (Gd), which is charged and distributes inversely to the PG content in the tissue. This inverse distribution of the Gd content enables the mapping of the cartilage glycosaminoglycan (GAG) content by the acquisition of the before and after images (17,18).

Since articular cartilage is a load-bearing tissue, it is important to understand the tissue properties as the function of external loading in order to better detect and manage the cartilage degradation (19–22). Given the fact that the mechanical modulus of articular cartilage is strongly depth-dependent (23), external loading of an intact specimen of articular cartilage will cause different amounts of compressions at different tissue depths, more in the surface portion and less in the deep portion of the tissue. To fully grasp the early degradation of articular cartilage (which tends to be small and localized), it is important to comprehend the topographical distributions of the cartilage properties at different tissue zones (depths) and different tissue locations. Such detailed information, especially important to the clinically important joints such as the tibia plateau in a knee joint, is largely lacking. This deficiency is probably not surprising, since articular cartilage is a thin layer of tissue (typically 0.5–3.5 mm, depending upon the particular joint) and the zonal measurement requires microscopic resolution in MRI, which most clinical MRI does not possess.

Microscopic MRI (μMRI) was used to study small blocks of canine cartilage-bone specimens from various locations of the medial tibial surface. Like human tissue, canine

articular cartilage has poor intrinsic healing ability. Canine tibia-femoral joint is relatively exposed and suited for studying the tissue damage and repair (20). However, the thickness of canine cartilage is thinner than humans, which the high spatial resolution of μMRI becomes extremely beneficial. In this project, the 17.6-μm transverse resolution of μMRI was adequate for resolving the complex features of the cartilage depth. We aimed to quantify both topographical and zonal variations of the load-induced changes in the tissue properties non-invasively, utilizing the strain-dependencies of both T1 and T2 relaxation times (20,21,24–26). Quantitative knowledge of the topographical responses of cartilage's macromolecule matrix to external loading, in a depth-dependent manner, could improve our understanding of the tissue's resistance to external forces, the lack of the resistance signaling the onset of the tissue degradation and the failure of the joint as a musculoskeletal organ.

Materials and methods

Sample preparation

Seven skeletally mature and healthy dogs (three females and four males, weighing ~19–32 kg) were sacrificed for a complex project, which was approved by the institutional review committees. Each medial tibial plateau was divided into five rectangular specimens (Figure 1). Each specimen was ~3.0 mm× 2.5 mm× 4~5 mm in size and included the full thickness of articular cartilage still attached to the underlying bone. These specimens were immersed in physiological saline (154 mM NaCl in deionized water) that contained 1% protease inhibitor cocktail (Sigma, MO) at 4 °C until imaging (never frozen). To prepare for imaging, a specimen was sealed in a precision glass tube with an internal diameter of 4.34 mm (Wilmad Glass, Buena, NJ), which was placed at room temperature (~20 °C) for ~4h. A total of 70 specimens from the 14 medial tibias were imaged without loading; 61 out of the 70 specimens were re-imaged under static loading in a homemade loading device. The loading device consists of two pieces of hard plastics, which can sandwich the specimen in between (20). The specimen can be compressed in various amounts by the means of plastic micro fasteners. The assembled device, together with the specimen, can be inserted into a 5-mm diameter NMR tubes for MRI experiments.

MRI protocols

μMRI experiments were performed using a Bruker AVANCE II 300 NMR spectrometer that has a vertical bore superconducting magnet (7 T/89 mm) and micro-imaging accessory (Bruker Instrument, Billerica, MA). A homemade 5 mm solenoid coil was used in all experiments. Using the magnetization-prepared imaging sequences (11), T1-weighted images were acquired at the magic angle (55°), which could minimize dipolar interaction to spin relaxation, and T2-weighted images were acquired at two orientations (0° and 55°) with respect to the external magnetic field B_0, in both the unloaded and loaded conditions. For any one specimen, all images were acquired at the same slice location of the specimen. In order to accurately determine the region of interest in imaging, a coronal pilot image was taken to position the slice location and a sagittal pilot image was taken to align the articular surface of cartilage to the desired orientation. The general imaging parameters were kept constant in all experiments: the field of view was 0.45 cm × 0.45 cm; the imaging matrix was 256 × 128; the inplane pixel size in the direction of the cartilage depth was 17.6 μm; the

slice thickness was 0.8 mm; the repetition time was 1.5 or 0.5 s and the experimental time was 6.5 or 2 h for the before or after Gd-soaked T1 experiments, respectively; the number of accumulations was 12; and the echo time was 7.2 ms.

The T1 experiment followed the high-resolution approach of the dGEMRIC procedure (17), where T1b refers to the data when the specimen was in equilibrium in the physiological saline solution, and T1Gd refers to the data when the specimen was in equilibrium in 1 mM gadolinium solution (Magnevist, Berlex, NJ). For any single experiment, T1-weighted images used an inversion recovery imaging sequence with five inversion points (without Gd: 0, 0.4, 1.1, 2.2, 4.0 s; with Gd: 0, 0.1, 0.3, 0.5, 1.0 s); T2-weighted images used a spin echo imaging sequence, where the echo time of the contrast segment had five increments for both at 0° and 55° (unloaded: 2, 8, 20, 40, 80 ms; loaded: 2, 18, 40, 80, 120 or 2, 18, 40, 70, 100 ms) and imaging time was 1.2 h. Both T1 and T2 images were calculated by a single exponential decay on a pixel-by-pixel basis. The quantitative images of Gd-$(DTPA)^{2-}$, fixed charged density (FCD) and GAG concentration in the cartilage were calculated using the T1 images based on a set of three equations (27,28).

$$[Gd]_t = \frac{1}{R} * \left| \frac{1}{T1Gd} - \frac{1}{T1b} \right| \quad (1)$$

$$FCD = [Na^+]_b * \left(\sqrt{\frac{[Gd]_t}{[Gd]_b}} - \sqrt{\frac{[Gd]_b}{[Gd]_t}} \right) \quad (2)$$

$$[GAG]_t = -\frac{502.5}{2} * [FCD] \quad (3)$$

where T1b and T1Gd are the T1 values before and after the Gd-soaked, respectively; $[Gd]_t$ and $[Gd]_b$ are the Gd concentrations in tissue and bath (soaking solution), respectively; R is the relaxivity of the Gd ions in saline; $[Na^+]_b$ is the sodium concentration in the bath; FCD and $[GAG]_t$ are the fixed charged density and the GAG concentration in tissue, respectively; "-", "2" and "502.65" in Equation (3) are the estimates from the assumption that there are 2 mol of negative charges per mole of disaccharide with a molecular weight of 502.5 g/mol.

Since, the relaxivity (R) of the Gd ions is a function of the solid concentrations in a system. It is common in the literature to estimate the R values of the tissue using a phantom (28), where the solid concentration can be varied. In this project, the R values of articular cartilage during loading was calculated based on the previous result (28), using Equation (4).

$$R = 4.17 + 0.08 \times \left| \frac{100 - \text{Watercontent}}{100 - \text{strain}} \right| \% \quad (4)$$

Together, the total imaging experiments from all unloaded and loaded specimens were 350 and the all experiments were performed within 8 days of the sacrifice.

Biomechanical protocol

Before harvesting the individual specimens from the tibia, a single step indentation experiment was performed with ~10 g load by manual control on all 14 intact joints, at the five locations on each medial tibia where the future imaging specimens would be harvested (Figure 1). The testing used a 5-mm diameter round-tip indenter attached to the actuator of an EnduraTec ELF 3200 system (Bose Corporation, Eden Prairie, MN). A joint was secured to a multi-axial rotational table vise, which allowed the precise positioning of the testing location to ensure perpendicularity between the cartilage surface and the indenter. The indenting phase was used to determine the compressive elastic modulus of each location. Since the ramp rate was manually controlled, a precise loading rate was difficult to obtain and varied between each test. To obtain the loading rate, a linear fit was carried out through the load-time data of each test. The slope of the fitted line, in units of grams per second, was used for the loading rate. To calculate the compressive elastic modulus, the force was plotted as a function of displacement and fitted linearly through the data points. The slope of the fitting, in units of Newtons per millimeter squared, and the cartilage thickness from MRI experiments were used to estimate the compressive elastic modulus at the testing location using the equation proposed by Hayes (29). Since the indentation rate was generally between ~2 and 10 g/s, an assumed Poisson's ratio of 0.5 (30) was chosen to simulate an incompressible material. This also simplified calculations since Poisson's ratio was not measured.

Water content protocol

Water content was measured from five skeletally healthy and mature dogs that were used for an unrelated study. These dogs came from a source that had provided us with the nearly identical tissues for over 10 years. The specimens were harvested using the identical procedures as described earlier. From each cartilage-bone specimen, the cartilage was carefully cut at the tissue-bone interface and placed back in a vial for hydration with saline. Then on a damp kimwipe tissue paper, the excess water around the tissue block was wiped off. The tissue was carefully weighed three times to estimate the experimental uncertainty. It was then dried in an oven for several days until a constant dry weight was achieved. With the wet and dry weight measurements, the water percentage was calculated.

Data and statistical analyses

To facilitate the quantitative comparison, a 10-pixel-wide region of interest was determined in image analysis in all 2D T2, T1 and GAG images of all specimens, from which 1D profiles were calculated. For the same specimen, the data were extracted from the same location of all 2D images. The total thickness of the tissue was measured from the T2 intensity images at 55° and normalized in order to compare the varying profiles among the specimens. The zonal boundaries were determined from the T2(0°) profiles, according to the criteria established and validated previously (31,32). The RZ was further divided into two equal halves (upper RZ1 and lower RZ2) for more accurate comparison. The bulk and zonal T2, T1 and GAG values were averaged within the selected zonal regions for each specimen.

All data from the 61 loaded specimens were analyzed for its bulk load-dependence; 19 of the 61 specimens were further analyzed for its zonal load-dependence. The strain level of each specimen was determined by measuring the difference in the full-thickness tissue before and after the cartilage was loaded. The location of the region of interest in image analysis between the unloaded and loaded cartilage images of each specimen was identical, which ensures an accurate determination of the strain-induced values. The ratio of the parameter changes was defined as $Ratio_i$:

$$Ratio_i = \left| \frac{V_{i\mathrm{L}} - V_{i\mathrm{UL}}}{V_{i\mathrm{UL}}} \right|$$

where i was the parameter to be analyzed [e.g. T2(0°), T2(55°), T1a, GAG and thickness], UL and L represent the cartilage unloaded and loaded, respectively. The values of $Ratio_i$ were plotted with strain, and the slopes and correlation r values were measured.

One-way ANOVA with Bonferroni correction was performed to test the differences: (1) among the five locations to determine the topographical variations of each tissue parameter at each independent tissue zone as well as bulk and (2) among sub-tissue zones to determine the zonal variations of each tissue parameter at each of the five locations. Then, to simplify the complex data, a Student's t-test was used to compare the meniscus-covered and the uncovered areas at each zone and bulk per parameter independently. Furthermore, to determine the topographical and zonal variations due to the external loading, a paired Student's t-test was performed between the mean of each parameter before and after loading at each zone and bulk at the meniscus-covered and uncovered areas. A p value of <0.05 was considered an indication of statistical significance and a p value of <0.001 was considered an indication of high statistical significance.

Results

Morphology observations

The meniscus on every joint was intact; both layers of the femoral and tibial cartilage appeared smooth with no visible evidence of damage. Each cartilage-bone specimen was first imaged in its coronal slice [Figure 2(a) (unloaded) and c (loaded)], which was used to determine a sagittal slice (Figure 2b) at which all subsequent experiments were carried out. The sharpness of these intensity images was notably influenced by the variations of the tissue within the 0.8-mm imaging-slice. The averaged thickness of the meniscus-covered specimens (AMT, EMT and PMT) was found to be ~ 30% thinner than that of the meniscus-uncovered specimens (CMT and IMT). Figure 3 showed a set of the quantitative T1, T2 and GAG images from one specimen under 0% and ~28% strains, respectively. The difference in the unloaded T2 images between 0° and 55° was the typical laminar appearance of cartilage in MRI. At the magic angle (55°), the loaded T2 images of articular cartilage could appear inhomogeneous, which was more notable at the edges of the specimens. Such appearance of being darker at edges and brighter in middle was more profound with high strain levels at CMT and IMT.

The depth-dependent profiles of cartilage

Figure 4(a) is a set of the unloaded T2 profiles at both 0° and 55° in the absolute scale in micrometers, which have the usual features as seen from these T2 results. Figure 4(b and c) show a representative set of the loaded T2 profiles from the same regions of interest in the same specimen at two orientations (0° and 55°) and two strains (0% and ~28%). Without the loading (•), the T2(55°) profile (Figure 4b) is relatively homogeneous without a distinctive peak while the T2(0°) profile has the usual single peak, centered at the TZ (Figure 4c). When the tissue was loaded (□), the upper portion of the T2(55°) profile reduces more than the lower portion of the profile (Figure 4b) and the T2(0°) peak shifted toward the deeper part of the tissue (Figure 4c). The shifting of the T2(0°) peak confirms the previous observation on the canine humeral cartilage (20), while the double peak at the T2(55°) was confirmed only for a few high strain T2 profiles in this project (not shown).

The calculated GAG profiles of the same specimen were shown in Figure 4(d), when the tissue was not loaded and loaded at ~28% strain. Several features are clearly visible in the GAG profiles. First, the GAG profile when the tibial cartilage was not loaded has an increasing trend from the surface to the radial zone, which is similar to the features in the humeral cartilage (17). Second, the GAG concentration in the loaded tissue increased significantly, both as the function of tissue depth and as the function of mechanical strain. Third, the initial portion of the cartilage (SZ and TZ) has the largest increase in GAG, as much as 110% at SZ, 90% at TZ, 30% at RZ1, 20% at RZ2 and ~30% averaged over the entire profile.

Topographical variations of the zonal properties of unloaded cartilage

To facilitate the statistical comparison among all imaging data, the cartilage depth profile was divided into four subtissue zones: SZ, TZ, RZ1 and RZ2. The zonal division was based on the profile of T2(0°), as shown in Figure 4(a) (13,28). Table 1 shows both the topographical and zonal variations of MRI parameters in articular cartilage from the medial tibias, when the tissue was not loaded. Zonal wise, the values of T2(0°) had a typical bell-curved shape as shown in Figure 4(a) (TZ>SZ>RZ1>RZ2) except at CMT (SZ>TZ>RZ1>RZ2); the values of T2(55°) were more homogeneous than those of T2(0°) and the values of both T1Gd and GAG had an increasing trend monotonically from SZ to RZ2. Not included in Table 1, the averaged values of the unloaded T1b on all locations were also measured: T1b(AMT) = 1.29 ± 0.05 s, T1b(EMT) = 1.22 ± 0.01 s, T1b(PMT) = 1.20 ± 0.15 s, T1b(CMT) = 1.46 ± 0.09 s and T1b(IMT) = 1.21 ± 0.23 s. In addition, the averaged bulk-GAG concentration was measured as 68.9 ± 8.0 mg/ml, which was the average of 19 specimens from three additional skeletally healthy and mature dogs for a different histochemical study.

To simplify the complex data, the five topographical regions were grouped into two areas, the meniscus-uncovered area (UC) and the meniscus-covered area (C). Table 2 shows the consolidated data with the results of the Student's *t*-test between the two areas. Most parameters from each sub-tissue zone as well as the total tissue (bulk average) were statistically significant or highly significant, except T2(0°) at RZ1 ($p = 0.414$), T2(55°) at SZ

($p = 0.058$), and GAG content (μg) at RZ1 ($p = 0.563$). Several conclusions could be drawn from this table.

- The tissue thickness: The two surface zones (SZ and TZ) in the covered area were thicker than the uncovered area, and vice versa at the two radial zones. This was true for both the absolute thickness and the relative thickness. In contrast, the total thickness (all zones) of the uncovered area was thicker than the covered area, since the radial zones are much thicker than the surface zones.
- T2(0°): The covered tissue had lower values than the uncovered ones in three of the four zones, except at RZ1 where T2 in two areas were the same. The trend in the bulk T2(0°) was the opposite – the covered area was higher than the uncovered area.
- T2(55°): The covered tissue had lower values than the uncovered ones in three of the four zones, except at SZ where T2 in two areas were the same. The trend in the bulk T2(55°) was the same.
- T1Gd: The covered tissue had higher values than the uncovered tissue, which were significant at all zones as well as the bulk average.
- GAG concentration (mg/ml): The covered tissue had higher values than the uncovered tissue, which were significant at all sub-tissue zones as well as the bulk. These trends are consistent with the slope of the modulus-rate plot, where the slope of the covered tissue had markedly higher that the uncovered tissue.
- Total GAG (μg): The two surface zones (SZ and TZ) in the covered area had higher values than the same zones in the uncovered area, and vice versa at the two radial zones and the bulk average.
- Water content: The covered tissue (63.3 ± 9.3%) was significantly lower than that of the uncovered tissue (73.2 ± 5.6%).

Averaged strain dependencies of the zonal properties of cartilage

Because of the depth-dependent mechanical modulus in articular cartilage, different zones should have different responses to external loading. Because of the topographical variations of the unloaded cartilage (as in Table 2), the response of the individual zones to external loading should also be topographically different. Table 3 summarizes the strain-dependent cartilage properties averaged from all five topographical locations and only from the paired data (i.e. each set of the unload and loaded data were from the same specimens). Several strain-dependent changes of the zonal properties of the tissue can be seen clearly.

- The tissue thickness: The SZ and TZ increased when loaded in both absolute thickness (8.2% and 24%) and relative thickness (24% and 52%), while the RZ1 and RZ2 decreased when loaded in both absolute thickness (32% and 34%) and relative thickness (9% and 11%).
- T2(0°) and T2(55°): The values in all zones as well as the bulk decreased when loaded. (T2(0°): 34% at SZ, 19% at TZ, 21% at RZ1, 19% at RZ2, 9% for the

bulk; T2(55°): 37% at SZ, 25% at TZ, 19% at RZ1, 10% at RZ2, 16% for the bulk).

- T1Gd: The values in the first three zones as well as the bulk increased when loaded (56% at SZ, 48% at TZ, 15% at RZ1 and 13% for the bulk). The values at RZ2 decreased by a small amount (2%) when loaded.
- GAG concentration (mg/ml): The values in all zones as well as the bulk increased when loaded (108% at SZ, 99% at TZ, 42% at RZ1, 19% at RZ2 and 42% for the bulk).
- The total GAG (μg): The values of the two surface zones (SZ and TZ) increased (152% and 139%) while these of two deep zones (RZ1 and RZ2) decreased (5% and 20%) when loaded. These trends are consistent with the depth-dependent zonal thickness in cartilage.

Topographical variations of the zonal properties of cartilage when loaded

Since each specimen was loaded manually when it was being imaged by μMRI, the amount of tissue loading was not the same for all specimens. To determine the topographical variations of the zonal properties of cartilage when it is being loaded, all paired imaging data (unloaded versus loaded) were analyzed together using the linear regression correlation method, as the strain-dependent ratios ((Load–Unload)/Unload). Figure 5 shows the ratios of the GAG changes in both the meniscus-covered and uncovered areas. In these linear regression plots, a larger slope indicates a stronger dependence on the strain; a narrower pair of the dashed lines (the 95% confidence lines) indicates less scattering of the data; and a positive or negative sign indicates the measurement increases or decreases with the strain. All other measurements (relative thickness, T2(0°), T2(55°), T1Gd) were analyzed in the same manner (the plots not shown). All slopes and r values of the correlation analysis were summarized in Tables 4 and 5, where each point represented one data set. Several features can be identified from these correlation analyses.

- The relative thickness: The uncovered area had higher slopes when compared to the covered area at all sub-tissue zones. The positive slopes in the SZ and TZ indicate an increase in the thickness; the negative slopes in the RZ1 and RZ2 indicate a decrease in the thickness. The larger increases in the uncovered tissue are consistent with the smaller GAG concentrations in this region (c.f., the GAG measurements in Table 2).
- T2: The tissue loading caused a reduction in T2 values in the bulk and all sub-tissue zones at both 0° and 55° (c.f., Figure 4b and c), which is consistent with the understanding that T2 is sensitive to the water content in the tissue.
- T1Gd and GAG concentration (mg/ml): The tissue loading caused an increase in T1Gd in the bulk and all sub-tissue zones (c.f., Figure 4d), which is consistent with the recent findings in the canine humeral cartilage regarding the compromised nature of several competing effects when a Gd-soaked tissue is compressed (26).

- GAG (μg): The changes in the zonal averaged GAG content varied and the surface portion of the tissue had the largest increases in the zonal GAG content. The trends of the strain dependencies of GAG content was: SZ>TZ>RZ1>RZ2. In contrast to the zonal GAG content, the total GAG in the bulk tissue stayed constant, regardless of the strain, which was indeed the case as shown in Figure 6, where the slopes were approximately unity. The total GAG in the tissue when averaged over the entire profiles were 11.6 ± 7.1 μg before loading and 11.7 ± 6.4 μg after loading ($p = 0.602$).

Discussion

This study demonstrates that significant variations in the biochemical and morphological properties of articular cartilage exist topographically over the healthy canine tibial plateaus. The use of μMRI was able to resolve at high resolution a number of MRI/tissue parameters of cartilage quantitatively and non-destructively. Furthermore, the use of static loading during the imaging was able to resolve the strain-dependencies of several tissue properties. The fact that mechanical loading of cartilage can alter the characteristics of MRI/tissue properties provides new insights to better understand the load-bearing performance of articular cartilage in human, which worsens *prior to* the onset of the clinical lesions in joints.

Topographical variations of the bulk tissue properties over the medial tibia

The bulk properties of articular cartilage are known to have significant topographical variations at different sites of a single joint surface. Among the properties that are known to vary include the water content between the meniscus-covered and exposed areas, the collagen fibril orientation of cartilage, the stiffness of cartilage in different animals, many physical and optical properties of cartilage by different modalities of tissue imaging, and the volume and thickness of cartilage in knee joints (7,29–32).

In this project, several cartilage properties were found to have topographical variations over the medial tibial surface. These variations were more pronounced when one divides the surface into two areas – the meniscus-covered area (AMT, EMT, PMT) and the uncovered area (IMT, CMT), which are summarized in Tables 1 and 2. For example, the cartilage in the covered area had lower water content, a thinner total thickness, a higher GAG concentration and a higher mechanical modulus. These trends are mutually consistent, and also consistent with the findings in the literature (29,33–35). In addition, the T2(55°) values are lower in the covered area, which agrees with the trend in the μMRI GAG concentration.

Topographical variations of the zonal properties of cartilage

What are not commonly known in the literature are the topographical variations of the *zonal* properties of articular cartilage, in a topographically complex joint such as the tibia. Such information requires the knowledge of two critical pieces of information, the high-resolution depth profiles of the tissue and the criteria that sub-divide the profiles into the discrete zones. In this project, the division of the sub-tissue zones was based on the profiles of T2(0°) of the specimen (Figure 4a), which has been validated by a correlation study between μMRI and polarized light microscopy (31), and recently updated by a multi-modality correlation

study (32). The zonal division data shown in Table 1 (the first row, the relative thickness) showed clearly that the relative zonal thicknesses of SZ and TZ were higher in the covered area, which resulted in the lower relative thicknesses of the two radial zones. This individual histological zone-specific averaging and comparison method can be possible, only when a pixel size is smaller than the thickness of the thinnest sub-tissue zone. Using μMRI, each small pixel covers a uniform structure, and most importantly, when we average the pixels, we average them in different thicknesses within their zones, which cannot be done in lower resolution imaging.

In this study, several topographical variations of the zonal properties of the medial tibial cartilage have been quantified by μMRI. As illustrated in Table 2, most differences between the covered and uncovered areas are significant. The weakest correlations are for the values of T2(0°), which is known to be strongly influenced by the dipolar interactions (11). It is interesting to note that some of the topographical variations of the zonal properties match the variations of the bulk properties, while some others do not. For example, the zonal distributions of the GAG concentration match the bulk property, i.e. the covered area has a consistently higher GAG concentration in all topographical sites, which agrees with the finding of Samosky et al. (33) in their T1Gd experiments. By comparison, the zonal distributions of the T2(0°) values had a less clear matching, which could be due to a variable degree of residual dipolar coupling that is common in T2 experiments.

Topographical variations of the zonal properties of loaded cartilage

The primary function of articular cartilage is its ability to bear load, which is mechanistically determined by the complex relationships among the molecular concentrations/structures and the interactions among the molecular constitutions in the extracellular matrix in the tissue. While the effects of loading on bulk cartilage thickness or volume have been investigated (36,37), the effect of loading on the zonal properties in cartilage is largely absent. Based on the knowledge of a strongly depth-dependent modulus in articular cartilage (23), it is reasonable to assume that the SZ of the tissue would deform larger and more easily than the RZ. The consequences of an external loading include the deformation of the collagen structures and a non-linear loss of the molecular constituents (water, ions) from the tissue. This load-bearing property of cartilage is measured in this imaging project as the load-induced changes, shown graphically in Figure 5 and summarized in Table 3 (the statistical analysis) and Tables 4 and 5 (the correlation slopes, whose absolute values are proportional to the rates of the changes and whose sign indicates a positive or negative change). Several trends can be found in this set of data.

Strain dependencies of the relative thickness—We observed that the relative thickness of the SZ and TZ of cartilage increased due to mechanical loading and that the relative thickness of the SZ and TZ of cartilage in the uncovered area increased more than the covered area. Consequently, these changes caused the relative thickness of the RZs to decrease in loading, differently for the covered and uncovered areas. This type of non-uniform deformations in cartilage has been observed in some early studies (34,35), where bulk compression on the tissue causes different strains at different tissue depths (23,38).

These results confirmed the collagen fibers were more deformed in the uncovered area than the covered area (36).

Strain dependencies of T2—T2 relaxation is sensitive to, among several other factors, the amount of water molecules and the orientation or packing of collagen fibers in the tissue. Loading on cartilage causes a number of structural modifications in cartilage such as exudation of water, decrease in water mobility, alteration of collagen fibril orientation, increasing molecular interactions and electrostatic forces. The higher loading causes shorter and more anisotropic T2 relaxation in cartilage, because the water is expelled from the cartilage tissue with loading and the amount of collagen is same in a smaller volume, which causes stronger couplings between water and macromolecules in cartilage. This is indeed the observation in this project, where all slopes for the T2 measurements (at both 0° and 55°) are negative (Tables 4 and 5). For the bulk T2, the slopes at the magic angle were steeper than those at 0°, which suggests that the highest sensitivity of T2 to loading occurs when the tissue is oriented at the magic angle. Because when the collagen fibrils in the cartilage tissue are oriented at the magic angle, the nuclear dipolar interaction in cartilage is minimized. In contrast, when the tissue is oriented at the 0°, the nuclear dipolar interaction has the most influence to spin relaxation, which could overshadow T2 reduction from loading. This result is also consistent with the findings in the literature (20,21,37,39,40). In addition, it is indicative that the superficial and transitional zones have the largest changes due to loading (Tables 4 and 5), which reflects again the depth-dependent mechanical modulus of the tissue. These load-induced trends of T2 relaxation could be used in both clinical diagnostics to detect the tissue softening due to lesions and mechanical testing to measure the tissue stiffness.

Strain dependencies of T1Gd and GAG—The values of T1Gd and GAG concentration were found to increase with the loading with significant correlation at each zone as well as bulk for both covered and uncovered areas, where the uncovered area seems to be affected more by strain than the covered area. For both covered and uncovered areas, the SZ and TZ had wider prediction intervals and higher slopes than RZs (Figure 5), which indicates that the GAG concentration at the surface tissue changes more and is more sensitive to loading than the RZs. This set of the results are consistent with an earlier finding from our lab that the value of T1 in the compressed cartilage could be reduced or increased, depending upon the concentration of the Gd ions in the solution (41). This knowledge is related to the clinical situations where the Gd transport was found to influence the interpretation of bulk dGEMRIC analysis *in vivo* human knee (42). This set of data demonstrates that the topographical variations of the zonal values of T1 in a structurally complex organ such as knee should be carefully examined in any quantitative effort to detect the local lesions in cartilage.

Total amount of GAG—Depth-wise, the averaged zonal GAG content increased at SZ and TZ and decreased at RZs significantly. It is clear that the surface portion of the tissue had the largest increases in the zonal GAG content since this part of the tissue is the softest and hence underwent more compression under a nominal overall stain. Consequently, this portion of the tissue would “gain” more GAG content when compressed. In contrast to the

zonal GAG content, the total GAG in the tissue should stay constant when the tissue is compressed, which is indeed the case (Figure 6). Overall, the total amount of GAG in μg is conserved before and after loading as we hypothesized that the total amount of the GAG in bulk cartilage would not be affected by loading, because the size of GAG molecules is too big to diffuse out of a healthy tissue during loading.

Experimental limitations and assumptions

There are several limitations and assumptions in this project that should be clarified. First, an averaged and strain-dependent T1b values was used instead of a strain-dependent T1b profile in the calculation of the GAG amount. As it is known, the T1b profile of articular cartilage is nearly isotropic and has minimal depth-dependency (11). Only a limited number of T1b experiments per block were performed in this project due to the time constraint. Second, we assumed that the macromolecules in cartilage would not diffuse out due to loading because of its large size. Third, the loading of the cartilage specimen in our MRI experiments was done manually. To compare the profiles and values of different samples, which would be under somewhat different strains, we calculated the data from various strains and made a fit to the plot of the parameter profile. Fourth, the loading rate of the bulk mechanical experiments (on the EnduraTec instrument) varied throughout each test, due to a manual control of the indenter displacement, i.e. the loading rate did not stay constant for an individual test. To account for this issue, an average load rate was calculated through regression line fitting of a stress-strain curve. Finally, although it is desirable to use a repetition time at least 2.5 times the T1 relaxation in MRI experiment, it is practically never possible in both the clinic (where the patient scan time is limited and patient movement needs to be minimized) and the lab research (when the total experimental time for all fresh specimens is limited). This shortened repetition time however does not affect the calculation of T1 and T2 relaxations in the magnetization prepared imaging sequences (11).

Conclusions

We demonstrated the significant topographical and zonal variations in the properties of canine tibial cartilage as the functions of external loading. These variations include the tissue thickness, T2, T1Gd and GAG. Significant correlation between the strain and cartilage properties demonstrates the potentials for high-resolution MRI experiments for biomechanical assessment. To the best of our knowledge, this is the first quantitative study of topographical and zonal variations of MRI parameters with different strains using μMRI at 17.6 μm resolutions. Since a softened cartilage deforms more under a fixed loading, quantitative knowledge of strain dependent regional and zonal variations of cartilage in knee joints can provide valuable insights to the evaluation of cartilage degradation and malfunction. Such detailed knowledge of the strain-modified MRI/tissue parameters would be great benefit for the diagnosis and possible future treatment of OA, and ultimately, in the prevention of articular diseases.

Acknowledgments

Declaration of interest

Y.X. is grateful to the National Institutes of Health for the R01 grant (AR 052353). The authors are indebted to Ms Janelle Spann (Michigan Resonance Imaging, Rochester Hills, Michigan) for providing the contrast agent, Dr M. Szarko (current address: University of London, UK) and Dr Nian Wang (current address: Duke University) for helping with the tissue harvest and experiments, Mr D. Mittelstaedt and Ms Carol Searight (both Dept of Physics, Oakland University) for editorial comments.

References

1. Benninghoff A Form und Bau der Gelenkknorpel in ihren Beziehungen zur Funktion. Erste Mitteilung. Zeitschrift für Anatomie und Entwicklungsgeschichte 1925;76:43–63.
2. Buckwalter JA, Mankin HJ. Articular cartilage: degeneration and osteoarthritis, repair, regeneration, and transplantation. Instr Course Lect 1998;47:487–504. [PubMed: 9571450]
3. Xia Y Averaged and depth-dependent anisotropy of articular cartilage by microscopic imaging. Semin Arthritis Rheum 2008;37:317–27. [PubMed: 17888496]
4. Weiss C, Rosenberg L, Helfet AJ. An ultrastructural study of normal young adult human articular cartilage. J Bone Joint Surg Am 1968;50:663–74. [PubMed: 5658553]
5. Xia Y Heterogeneity of cartilage laminae in MR imaging. J Magn Reson Imaging 2000;11:686–93. [PubMed: 10862069]
6. Jurvelin JS, Arokoski JP, Hunziker EB, Helminen HJ. Topographical variation of the elastic properties of articular cartilage in the canine knee. J Biomech 2000;33:669–75. [PubMed: 10807987]
7. Xia Y, Moody JB, Alhadlaq H, Hu J. Imaging the physical and morphological properties of a multi-zone young articular cartilage at microscopic resolution. J Magn Reson Imaging 2003;17:365–74. [PubMed: 12594728]
8. Brama PA, Holopainen J, van Weeren PR, Firth EC, Helminen HJ, Hyttinen MM. Influence of exercise and joint topography on depth-related spatial distribution of proteoglycan and collagen content in immature equine articular cartilage. Equine Vet J 2009;41:557–63. [PubMed: 19803051]
9. Armstrong CG, Mow VC. Variations in the intrinsic mechanical properties of human articular cartilage with age, degeneration, and water content. J Bone Joint Surg Am 1982;64:88–94. [PubMed: 7054208]
10. Buckwalter JA, Martin J. Degenerative joint disease. Clin Symp 1995;47:1–32. [PubMed: 7554763]
11. Xia Y Relaxation anisotropy in cartilage by NMR microscopy (muMRI) at 14-microm resolution. Magn Reson Med 1998;39:941–9. [PubMed: 9621918]
12. Fragonas E, Mlynarik V, Jellus V, Micali F, Piras A, Toffanin R, et al. Correlation between biochemical composition and magnetic resonance appearance of articular cartilage. Osteoarthritis Cartilage 1998;6:24–32. [PubMed: 9616436]
13. Xia Y, Elder K. Quantification of the graphical details of collagen fibrils in transmission electron micrographs. J Microsc 2001;204:3–16. [PubMed: 11580808]
14. Nissi MJ, Rieppo J, Toyras J, Laasanen MS, Kiviranta I, Nieminen MT, et al. Estimation of mechanical properties of articular cartilage with MRI – dGEMRIC, T2 and T1 imaging in different species with variable stages of maturation. Osteoarthritis Cartilage 2007;15:1141–8. [PubMed: 17513137]
15. Stikov N, Keenan KE, Pauly JM, Smith RL, Dougherty RF, Gold GE. Cross-relaxation imaging of human articular cartilage. Magn Reson Med 2011;66:725–34. [PubMed: 21416504]
16. Wiener E, Pfirrmann CW, Hodler J. Spatial variation in T1 of healthy human articular cartilage of the knee joint. Br J Radiol 2010;83:476–85. [PubMed: 19723767]
17. Xia Y, Zheng S, Bidthanapally A. Depth-dependent profiles of glycosaminoglycans in articular cartilage by microMRI and histochemistry. J Magn Reson Imaging 2008;28:151–7. [PubMed: 18581328]
18. Bashir A, Gray ML, Hartke J, Burstein D. Nondestructive imaging of human cartilage glycosaminoglycan concentration by MRI. Magn Reson Med 1999;41:857–65. [PubMed: 10332865]

19. Eckstein F, Faber S, Muhlbauer R, Hohe J, Englmeier KH, Reiser M, et al. Functional adaptation of human joints to mechanical stimuli. Osteoarthritis Cartilage 2002;10:44–50. [PubMed: 11795982]
20. Alhadlaq HA, Xia Y. The structural adaptations in compressed articular cartilage by microscopic MRI (microMRI) T(2) anisotropy. Osteoarthritis Cartilage 2004;12:887–94. [PubMed: 15501404]
21. Alhadlaq HA, Xia Y. Modifications of orientational dependence of microscopic magnetic resonance imaging T(2) anisotropy in compressed articular cartilage. J Magn Reson Imaging 2005;22:665–73. [PubMed: 16220547]
22. Brama PA, Holopainen J, van Weeren PR, Firth EC, Helminen HJ, Hyttinen MM. Effect of loading on the organization of the collagen fibril network in juvenile equine articular cartilage. J Orthop Res 2009;27:1226–34. [PubMed: 19242977]
23. Chen SS, Falcovitz YH, Schneiderman R, Maroudas A, Sah RL. Depth-dependent compressive properties of normal aged human femoral head articular cartilage: relationship to fixed charge density. Osteoarthritis Cartilage 2001;9:561–9. [PubMed: 11520170]
24. Chiu EJ, Newitt DC, Segal MR, Hu SS, Lotz JC, Majumdar S. Magnetic resonance imaging measurement of relaxation and water diffusion in the human lumbar intervertebral disc under compression in vitro. Spine 2001;26:E437–44. [PubMed: 11698903]
25. Lammentausta E, Kiviranta P, Nissi MJ, Laasanen MS, Kiviranta I, Nieminen MT, et al. T2 relaxation time and delayed gadolinium-enhanced MRI of cartilage (dGEMRIC) of human patellar cartilage at 1.5 T and 9.4 T: relationships with tissue mechanical properties. J Orthop Res 2006;24:366–74. [PubMed: 16479569]
26. Xia Y, Wang N, Lee J, Badar F. Strain-dependent T1 relaxation profiles in articular cartilage by MRI at microscopic resolutions. Magn Reson Med 2011;65:1733–7. [PubMed: 21452280]
27. Maroudas A, Muir H, Wingham J. The correlation of fixed negative charge with glycosaminoglycan content of human articular cartilage. Biochim Biophys Acta 1969;177:492–500. [PubMed: 4239606]
28. Zheng S, Xia Y. The impact of the relaxivity definition on the quantitative measurement of glycosaminoglycans in cartilage by the MRI dGEMRIC method. Magn Reson Med 2010;63:25–32. [PubMed: 19918900]
29. Hayes WC, Keer LM, Herrmann G, Mockros LF. A mathematical analysis for indentation tests of articular cartilage. J Biomech 1972;5:541–51. [PubMed: 4667277]
30. Mow VC, Gibbs MC, Lai WM, Zhu WB, Athanasiou KA. Biphasic indentation of articular cartilage – II. A numerical algorithm and an experimental study. J Biomech 1989;22:853–61. [PubMed: 2613721]
31. Xia Y, Moody JB, Burton-Wurster N, Lust G. Quantitative in situ correlation between microscopic MRI and polarized light microscopy studies of articular cartilage. Osteoarthritis Cartilage 2001;9:393–406. [PubMed: 11467887]
32. Lee JH, Xia Y. Quantitative zonal differentiation of articular cartilage by microscopic magnetic resonance imaging, polarized light microscopy, and Fourier-transform infrared imaging. Microsc Res Tech 2013;76:625–32. [PubMed: 23533143]
33. Samosky JT, Burstein D, Eric Grimson W, Howe R, Martin S, Gray ML. Spatially-localized correlation of dGEMRIC-measured GAG distribution and mechanical stiffness in the human tibial plateau. J Orthop Res 2005;23:93–101. [PubMed: 15607880]
34. Kiraly K, Hyttinen MM, Parkkinen JJ, Arokoski JA, Lapvetelainen T, Torronen K, et al. Articular cartilage collagen birefringence is altered concurrent with changes in proteoglycan synthesis during dynamic in vitro loading. Anat Rec 1998;251:28–36. [PubMed: 9605217]
35. Carballido-Gamio J, Stahl R, Blumenkrantz G, Romero A, Majumdar S, Link TM. Spatial analysis of magnetic resonance T1rho and T2 relaxation times improves classification between subjects with and without osteoarthritis. Med Phys 2009;36: 4059–67. [PubMed: 19810478]
36. Kaab MJ, Ito K, Clark JM, Notzli HP. The acute structural changes of loaded articular cartilage following meniscectomy or ACL-transection. Osteoarthritis Cartilage 2000;8:464–73. [PubMed: 11069731]
37. Rubenstein JD, Kim JK, Henkelman RM. Effects of compression and recovery on bovine articular cartilage: appearance on MR images. Radiology 1996;201:843–50. [PubMed: 8939241]

38. Schinagl RM, Gurskis D, Chen AC, Sah RL. Depth-dependent confined compression modulus of full-thickness bovine articular cartilage. J Orthop Res 1997;15:499–506. [PubMed: 9379258]

39. Mosher TJ, Smith HE, Collins C, Liu Y, Hancy J, Dardzinski BJ, et al. Change in knee cartilage T2 at MR imaging after running: a feasibility study. Radiology 2005;234:245–9. [PubMed: 15550376]

40. de Visser SK, Crawford RW, Pope JM. Structural adaptations in compressed articular cartilage measured by diffusion tensor imaging. Osteoarthritis Cartilage 2008;16:83–9. [PubMed: 17625926]

41. Wang N, Chopin E, Xia Y. The effects of mechanical loading and gadolinium concentration on the change of T1 and quantification of glycosaminoglycans in articular cartilage by microscopic MRI. Phys Med Biol 2013;58:4535–47. [PubMed: 23760174]

42. Hawezi ZK, Lammentausta E, Svensson J, Dahlberg LE, Tiderius CJ. In vivo transport of Gd-DTPA(2-) in human knee cartilage assessed by depth-wise dGEMRIC analysis. J Magn Reson Imaging 2011;34:1352–8. [PubMed: 21954084]

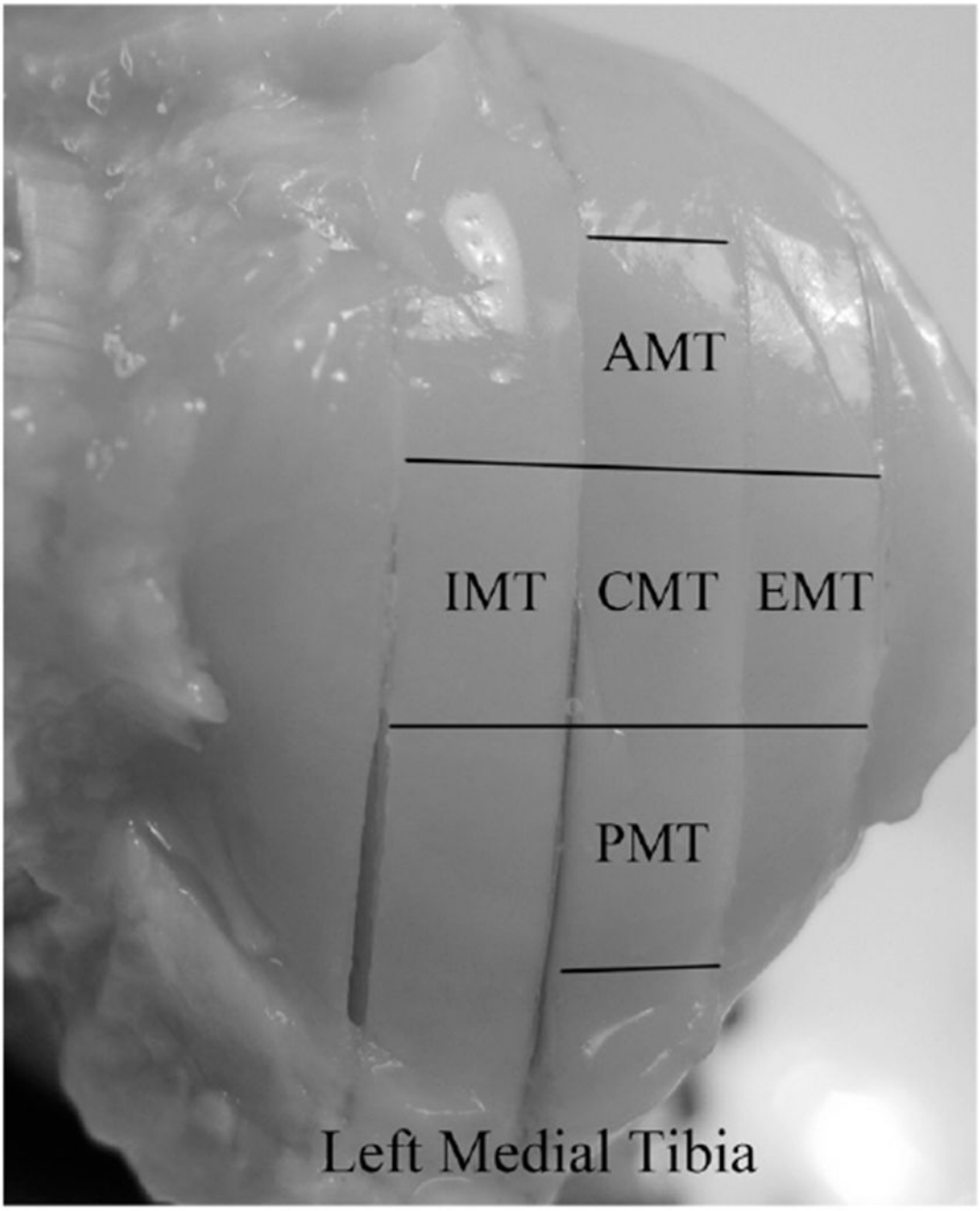

Figure 1.
The topographical locations of the specimens on the surface of a left medial tibia. In the meniscus-covered area, there are anterior medial tibia (AMT), exterior medial tibia (EMT) and posterior medial tibia (PMT) specimens. In the meniscus-uncovered area, there are central medial tibia (CMT) and interior medial tibia (IMT) specimens.

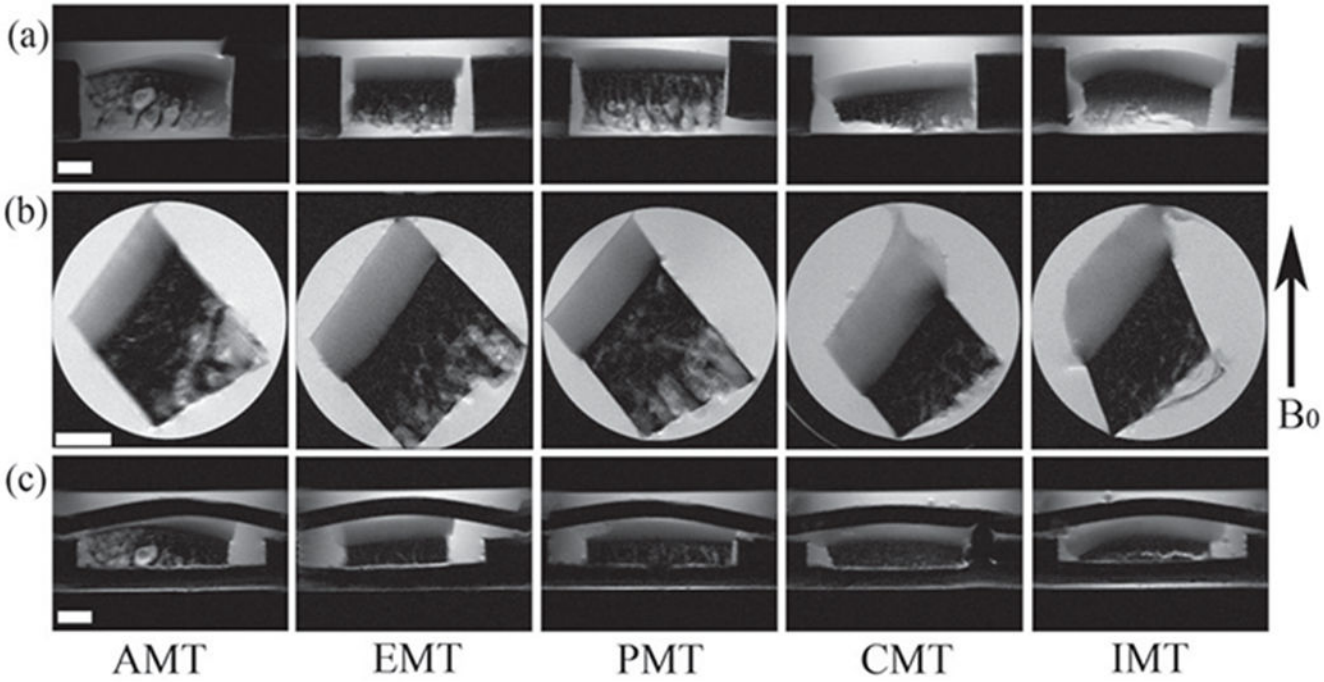

Figure 2.

(a) The coronal intensity images without loading, which are used to define the slice location of the subsequent sagittal images in (b). (c) The coronal intensity images under loading. The white bar indicates 1 mm. The display intensities of all images in the figure are the same.

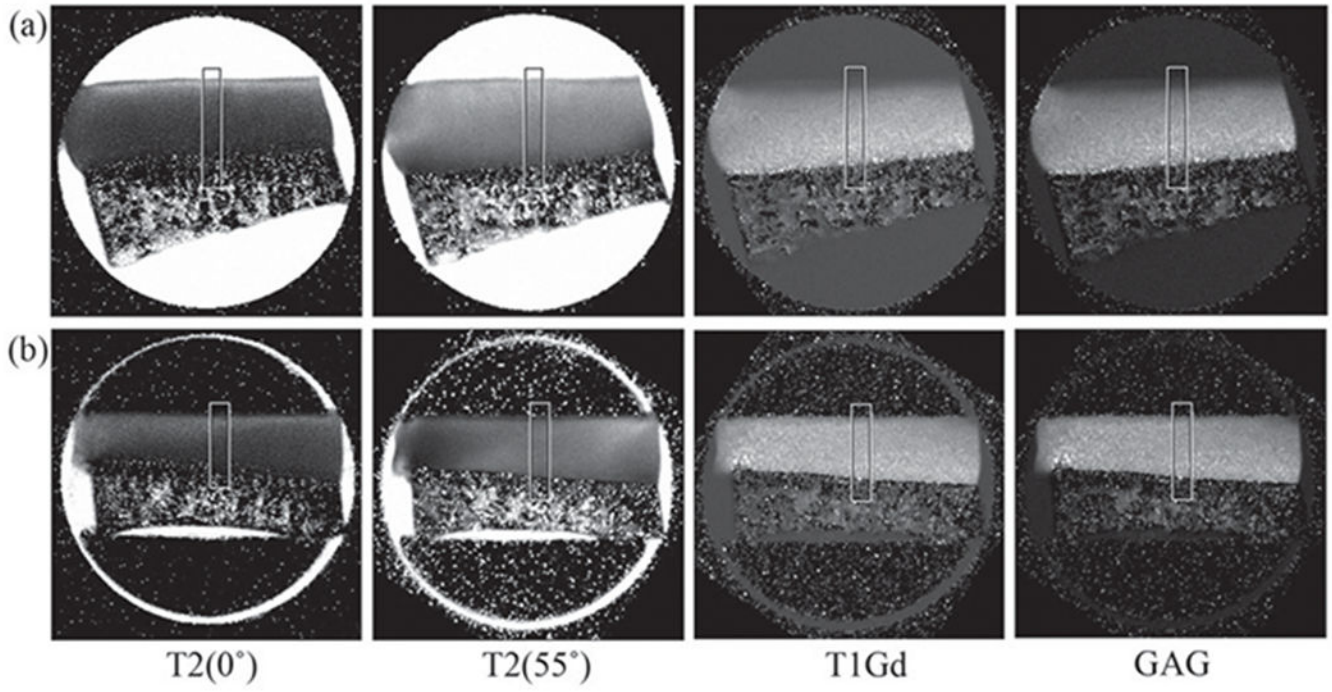

Figure 3.

Quantitative MRI images of a specimen without loading (a) and while loaded (b). The angle was defined as the angle between the articular surface of cartilage and the direction of the magnetic field (B_0). The T2(55°) and T1Gd images were acquired at 55° and rotated in the image analysis.

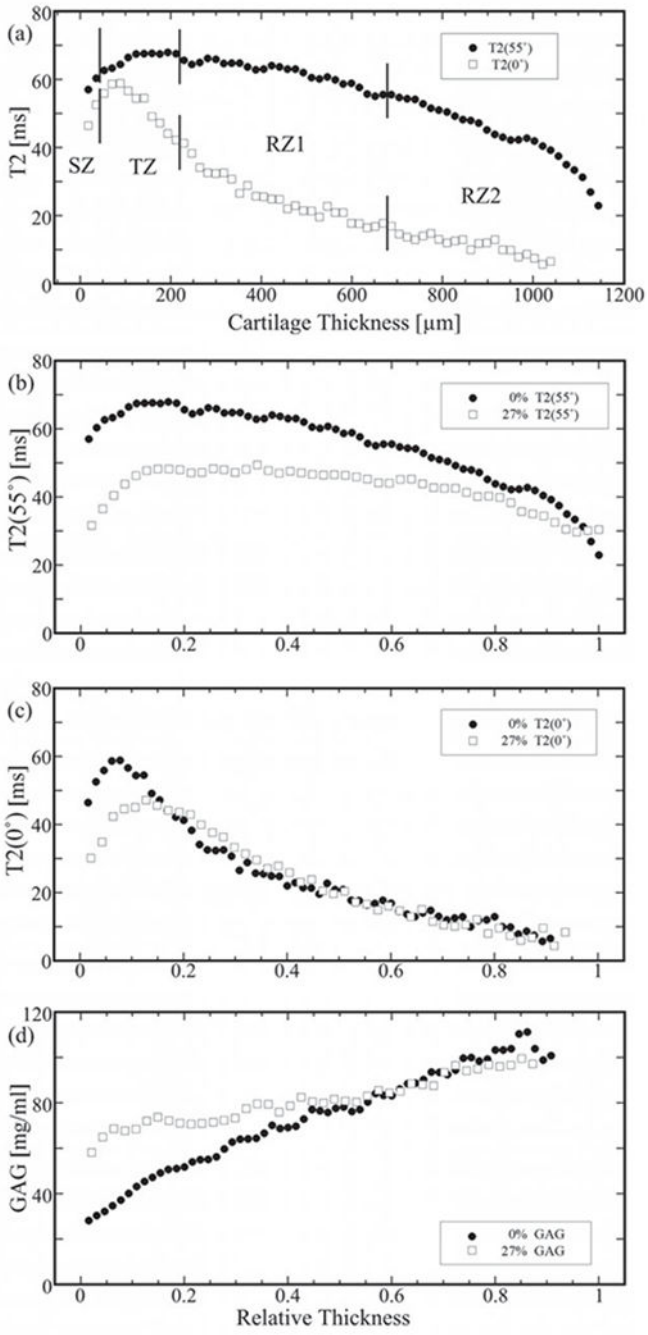

Figure 4.

A representative set of 1D μMRI profiles from a single specimen. (a) T2 profiles with zonal divisions at 0° (solid dots) and 55° (open squares). (b) T2 profiles at 55°. (c) T2 profiles at 0°. (d) GAG profiles. [In b and c, the solid dots are for the unloaded (UL) profiles and the open squares are for the loaded (L) profiles at the strain of 27.7% and the all profiles were normalized to compare the profiles of the UL and L, setting 0 at the surface and 1 at the cartilage-bone interface.].

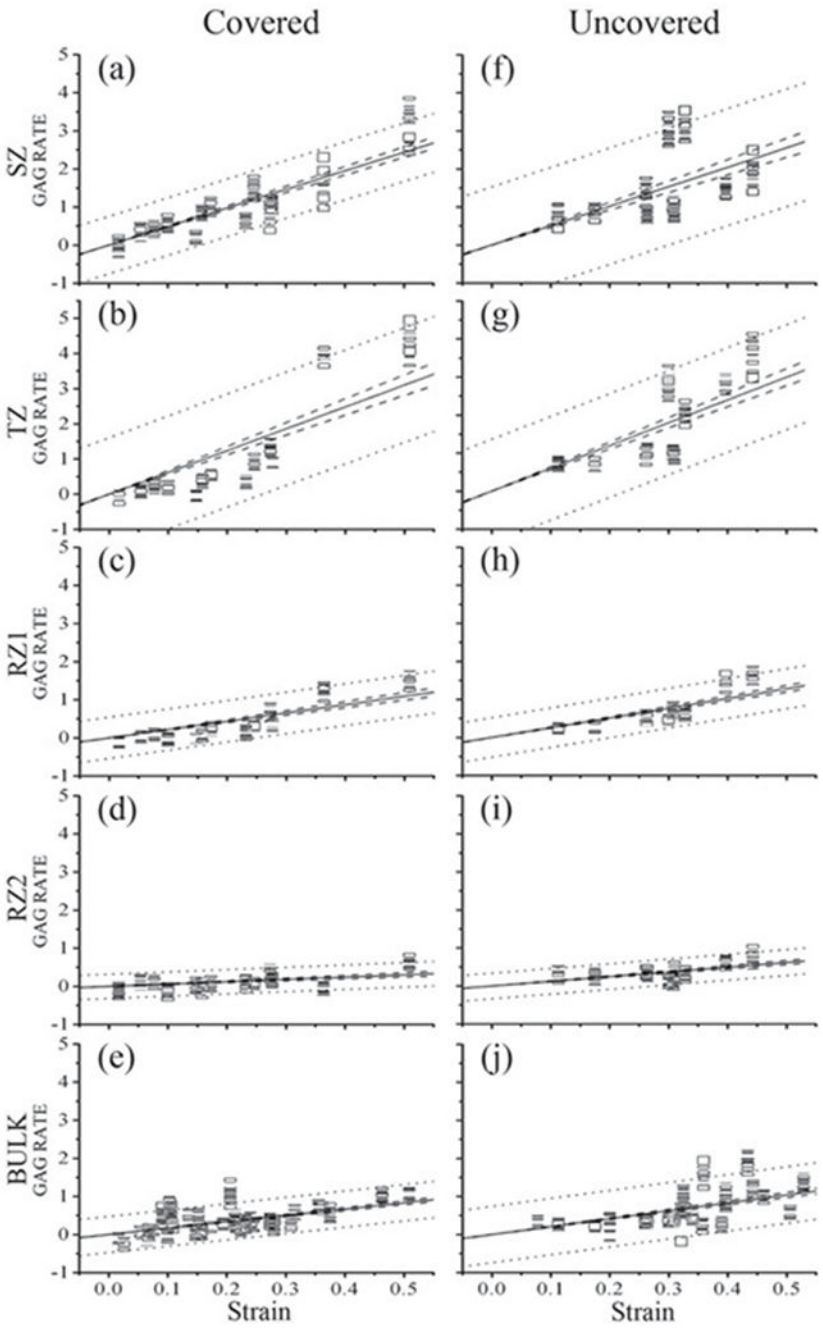

Figure 5.

A representative set of the load-induced changes of GAG ((L-UL)/UL) at different zones in the meniscus covered (left) and uncovered areas (right). Since SZ and TZ had wider prediction intervals and higher slopes than RZs, it can be predicted that the GAG concentration at the surface tissue could change more and be more sensitive to loading than the deep tissue. The dashed line showed the 95% confidence intervals and the dotted line showed the 95% prediction intervals.

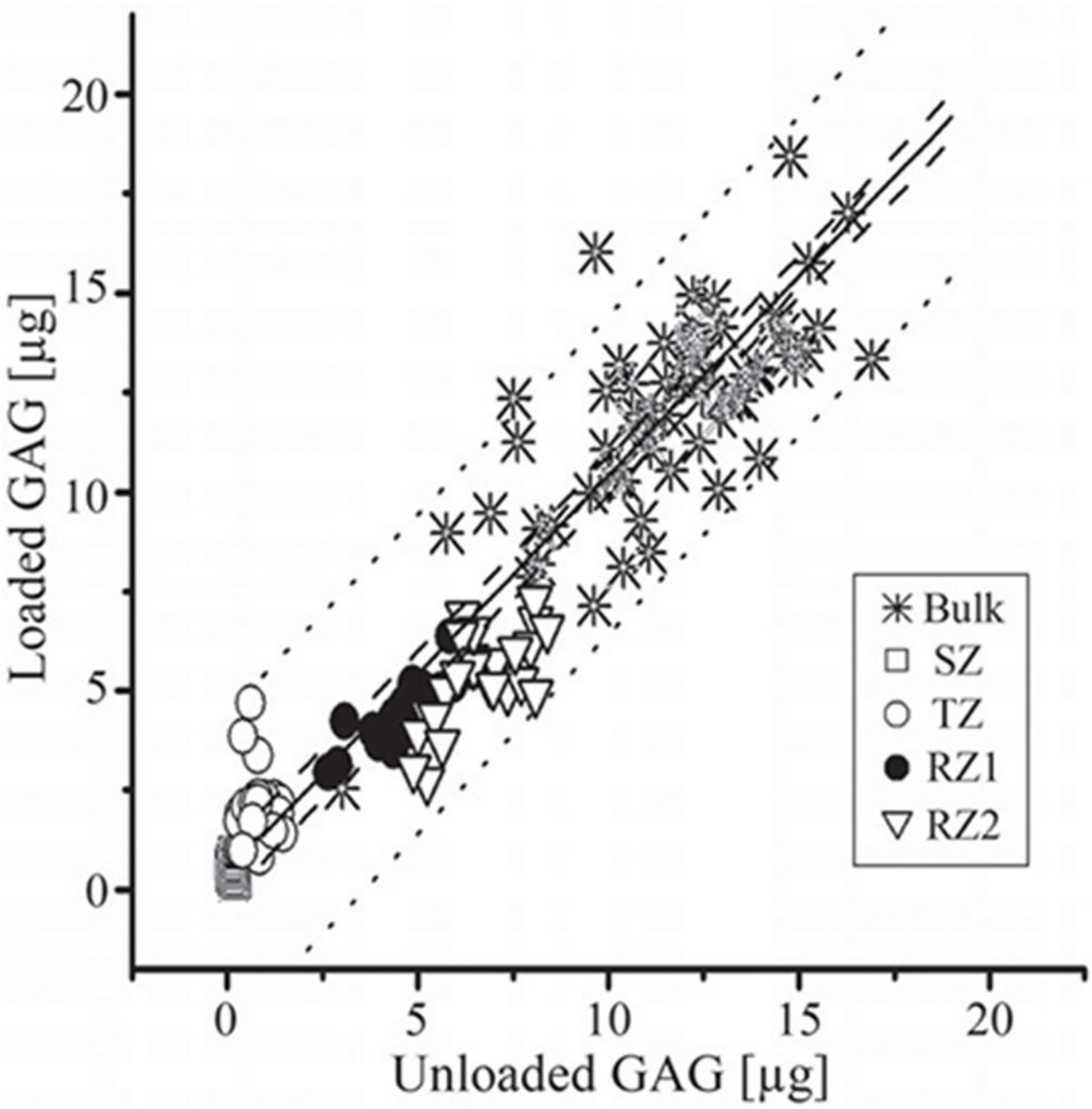

Figure 6.
The bulk and zonal contents of GAG (in mg unit) before and after the loading. The solid line showed the slope of 1, the dashed line showed the 95% confident intervals and the dotted line showed the 95% prediction intervals.

Table 1.

Topographical maps of different tissue parameters as the bulk values and in all sub-tissue zones.

	Bulk			SZ			TZ			RZ1			RZ2		
relative thickness [%]		AMT			4.6			13.2			41.5			40.8	
	IMT	CMT	EMT	2.9	2.6	3.1	9.4	12.9	15.6	44.4	42.5	40.9	43.4	42.1	40.5
		PMT			3.7			15.0			41.0			40.2	
absolute thickness [μm]		1014.9			46.2			138.6			414.7			408.1	
	1297.4	1216.9	892.1	40.2	28.9	35.2	111.9	154.6	157.3	577.0	519.2	353.1	568.2	512.9	346.5
		799.0			39.9			142.0			313.3			303.9	
T2-0 [ms]		24.3			49.5			52.7			21.2			8.8	
	20.0	25.8	28.0	44.1	60.0	54.0	50.1	58.8	55.9	20.4	25.2	24.9	9.4	10.3	9.9
		25.1			43.5			48.7			21.2			8.8	
T2-55 [ms]		45.1			57.1			58.9			48.9			33.8	
	50.5	51.6	39.8	45.8	64.2	49.0	55.2	69.5	51.6	57.8	60.7	42.9	41.9	35.4	28.9
		44.6			52.7			54.8			47.6			33.2	
T1a [s]		0.516			0.275			0.329			0.494			0.654	
	0.517	0.512	0.557	0.264	0.271	0.310	0.313	0.321	0.399	0.474	0.473	0.558	0.631	0.642	0.681
		0.535			0.317			0.396			0.547			0.638	
GAG [mg/ml]		80.9			36.6			46.8			77.0			107.4	
	69.9	69.1	91.3	28.1	29.3	44.5	36.9	38.1	61.2	63.1	63.0	91.4	88.2	90.0	118.4
		88.3			46.0			61.2			90.8			110.8	
Modulus (Biomechanics) [MPa]		1.627													
	1.033	0.713	1.669												
		1.868													
water content [%]		56.9													
	73.5	72.9	64.3												
		68.8													

Table 2.

Average values (±SDs) of parameters on the meniscus-covered (C) and uncovered (UC) regions.

	Absolute thickness (μm)			Relative thickness (%)			T2(0°) (ms)			T2(55°) (ms)			T1Gd (ms)			GAG (mg/ml)			GAG (μg)		
	C	UC	*p*	C	UC	*p*	C	UC	*p*	C	UC	*p*	C	UC	*p*	C	UC	*p*	C	UC	*p*
Bulk	907.6 (187.9)	1251.6 (218.4)	***				25.8 (4.5)	22.9 (5.3)	***	43.6 (8.1)	51.1 (8.5)	***	536 (79)	514 (58)	***	86.0 (15.3)	70.0 (8.8)	***	10.92 (3.23)	12.22 (1.98)	*
SZ	40.2 (8.8)	34.6 (10.8)	***	4.9 (2.2)	2.8 (1.0)	***	49.1 (13.1)	52.1 (13.6)	**	53.1 (12.5)	55.0 (13.8)	–	301 (60)	268 (31)	***	37.7 (10.8)	29.0 (5.4)	***	0.23 (0.09)	0.14 (0.06)	***
TZ	147.9 (30.1)	133.3 (25.2)	***	17.1 (5.3)	10.8 (3.0)	***	52.7 (9.6)	54.5 (10.9)	*	55.3 (12.0)	62.4 (13.8)	***	374 (80)	317 (46)	***	46.8 (15.8)	37.0 (6.5)	***	1.15 (0.42)	0.70 (0.20)	***
RZ1	356.2 (104.6)	548.1 (102.4)	***	39.5 (3.4)	43.5 (1.5)	***	22.5 (4.4)	22.8 (6.2)	–	46.8 (10.4)	59.3 (11.5)	***	533 (85)	473 (71)	***	79.3 (17.9)	62.3 (9.8)	***	4.29 (1.36)	4.80 (0.90)	–
RZ2	347.8 (104.7)	540.6 (150.8)	***	38.6 (3.5)	42.8 (1.7)	***	9.2 (2.0)	9.9 (2.7)	***	32.2 (7.4)	38.6 (7.2)	***	658 (81)	636 (60)	***	111.0 (15.5)	90.9 (7.7)	***	5.55 (1.85)	6.75 (1.28)	**

C: $N = 470$, UC: $N = 280$ for each parameter except GAG (μg) C: $N = 47$, UC: $N = 28$.

The statistical results of Student's *t*-test between C and UC of parameters (*$p<0.05$, **$p<0.01$, ***$p<0.001$; −$p>0.05$) are shown.

Table 3.

Average values (±SDs) of parameters before (UL) and after (L) loading (paired data only) with the bulk strain for the whole tissue was 24%; 20% for the covered tissue and 29% for the uncovered tissue.

	Absolute thickness (μm)			Relative thickness (%)			T2(0°) (ms)			T2(55°) (ms)			T1Gd (ms)			GAG (mg/ml)			GAG (μg)		
	UL	L	*p*	UL	L	*p*	UL	L	*p*	UL	L	*p*	UL	L	*p*	UL	L	*p*	UL	L	*p*
Bulk	1042.6 (176.3)	780.8 (140.5)	***				26.9 (3.9)	24.4 (4.7)	***	46.6 (8.3)	39.1 (7.4)	***	529 (72)	597 (90)	***	79.8 (15.3)	113.2 (26.6)	***	11.60 (2.67)	11.71 (2.52)	–
SZ	39.1 (11.6)	42.3 (15.3)	–	3.6 (1.2)	5.1 (2.0)	***	58.6 (10.7)	39.1 (8.9)	***	60.7 (10.1)	38.4 (11.0)	***	268 (35)	419 (96)	***	34.2 (10.0)	71.2 (22.4)	***	0.18 (0.06)	0.44 (0.25)	***
TZ	134.9 (25.9)	166.7 (33.2)	***	12.4 (3.3)	20.2 (3.8)	***	59.1 (7.6)	46.6 (10.7)	***	65.5 (10.7)	49.4 (11.9)	***	328 (66)	486 (108)	***	43.5 (13.8)	86.4 (29.5)	***	0.86 (0.39)	2.05 (0.90)	***
RZ1	475.4 (89.2)	321.1 (64.9)	***	42.4 (2.0)	38.0 (2.5)	***	25.8 (4.4)	20.6 (5.7)	***	51.4 (12.4)	47.5 (10.3)	***	489 (85)	562 (73)	***	71.9 (17.1)	102.3 (23.7)	***	4.70 (0.95)	4.49 (0.77)	***
RZ2	467.9 (88.7)	311.2 (66.8)	***	41.8 (2.2)	36.8 (2.7)	***	11.2 (2.0)	9.1 (2.2)	***	34.6 (7.9)	33.7 (6.2)	***	658 (62)	647 (63)	**	102.3 (16.1)	121.7 (17.9)	***	6.64 (1.12)	5.31 (1.22)	***

N = 470 for bulk, 230 for zone.

The statistical results of the paired Student's t-test between UL and L on parameters (*p<0.05, **p<0.01, ***p<0.001, −p>0.05) are shown.

Table 4.

Slope values of strain versus the ratio of the parameter changes for the meniscus covered (C) and uncovered (UC) regions.

	Relative thickness (%)		T2(0°) (ms)		T2(55°) (ms)		T1Gd (s)		GAG (mg/ml)	
	C	UC	C	UC	C	UC	C	UC	C	UC
Bulk			−0.429	−0.331	−0.673	−0.684	0.583	0.553	1.702	2.085
SZ	0.726	2.992	−1.216	−1.140	−1.573	−1.072	1.932	2.702	4.943	6.586
TZ	1.894	4.646	−0.923	−0.893	−1.005	−0.964	2.503	2.541	6.293	5.991
RZ1	−0.225	−0.563	−0.781	−1.051	−0.575	−0.936	0.870	0.883	2.198	2.562
RZ2	−0.225	−0.622	−0.621	−0.947	−0.104	−0.576	−0.139	0.073	0.619	1.232

Table 5.

Correlation r values of strain versus the ratio of the parameter changes for the meniscus covered (C) and uncovered (UC) regions.

	Relative thickness (%)		T2(0°) (ms)		T2(55°) (ms)		T1Gd (s)		GAG (mg/ml)	
	C	UC	C	UC	C	UC	C	UC	C	UC
Bulk			0.362	0.513	0.575	0.280	0.369	0.584	0.355	0.570
SZ	0.194[a]	0.199[a]	0.377	0.184	0.691	0.066[a]	0.738	0.526	0.899	0.467
TZ	0.684	0.769	0.808	0.494	0.713	0.471	0.873	0.665	0.898	0.640
RZ1	0.389	0.696	0.752	0.796	0.552	0.841	0.848	0.866	0.864	0.878
RZ2	0.389	0.760	0.384	0.666	0.021[a]	0.643	0.046[a]	0.017[a]	0.266	0.012[a]

[a]Not statistically significant correlated (correlation probability >0.05) between the strain and the ratio of the parameter changes from the paired Student's *t*-test. Otherwise, they were statistically significant correlated (correlation probability <0.05).